



Published in final edited form as:

Prostaglandins Other Lipid Mediat. 2018 January ; 134: 93–107. doi:10.1016/j.prostaglandins.2017.09.005.

HUMAN RETINAL ENDOTHELIAL CELLS AND ASTROCYTES CULTURED ON 3-D SCAFFOLDS FOR OCULAR DRUG DISCOVERY AND DEVELOPMENT

Kay D. Beharry, BS^{1,2,3}, Charles L. Cai, MD¹, Gloria B. Valencia, MD¹, Douglas Lazzaro, MD^{2,3}, Arwin M. Valencia, MD⁴, Fabrizio Salomone, PhD⁵, and Jacob V. Aranda, MD, PhD^{1,2,3}

¹Department of Pediatrics, Division of Neonatal-Perinatal Medicine, State University of New York, Downstate Medical Center, Brooklyn, NY, USA

²Department of Ophthalmology; State University of New York, Downstate Medical Center, Brooklyn, NY, USA

³SUNY Eye Institute, NY, NY, USA

⁴Henderson Medical Center, Henderson, NV, USA

⁵Chiesi Farmaceutici S.p.A., Parma, Italy

Abstract

Topical ocular ketorolac improves the outcomes of severe retinopathy of prematurity and when administered with systemic caffeine, decreases the severity of oxygen-induced retinopathy. We tested the hypothesis that co-cultures of human retinal endothelial cells (HRECs) and human retinal astrocytes (HRAs) on 3-dimensional (3-D) hydrogel scaffolds is a more representative biomimetic paradigm of the blood-retinal-barrier (BRB) than 2-D cultures, and should be utilized for preclinical drug discovery and development. Mono- and co-cultures of HRECs and HRAs were treated with standard doses of ketorolac, ibuprofen, and/or caffeine, and exposed to hyperoxia, intermittent hypoxia (IH), or normoxia on 2-D surfaces or 3-D biodegradable hydrogel scaffolds (AlgiMatrix or Geltrex). Media and cells were collected at 72 hours post treatment for arachidonic acid metabolites. Cells cultured on 3-D scaffolds exhibited less oxidative stress and variability in drug responses. HRAs enhanced the responses of HRECs to drugs and changes in oxygen environment. PGE₂ and PGI₂ were the predominant prostanoids produced in response to IH, reflecting COX-2 immunoreactivity. We conclude that HRECs and HRAs co-cultured on 3-D

Corresponding author: Kay D. Beharry, Research Assistant Professor, Department of Pediatrics & Ophthalmology, Director, Neonatal-Perinatal Medicine Clinical & Translational Research Labs, Dept. Pediatrics/Div. Neonatal-Perinatal Medicine, State University of New York, Downstate Medical Center, 450 Clarkson Avenue, Box 49, Brooklyn, NY, 11203, USA, kbeharry@downstate.edu, Tel: (718) 270-1475, Fax: (718) 613-8528.

Conflict of interest: The authors declare that they have no conflicts of interest related to this manuscript.

Financial Disclosure: The authors declare that they have no financial support relevant to this manuscript.

Publisher's Disclaimer: This is a PDF file of an unedited manuscript that has been accepted for publication. As a service to our customers we are providing this early version of the manuscript. The manuscript will undergo copyediting, typesetting, and review of the resulting proof before it is published in its final citable form. Please note that during the production process errors may be discovered which could affect the content, and all legal disclaimers that apply to the journal pertain.

scaffolds may recapitulate drug responses of the dynamic BRB and therefore should be implemented for preclinical ocular drug discovery and development.

Keywords

AlgiMatrix; Biodegradable 3-D Scaffolds; Caffeine; Co-Cultures; Geltrex; Human Retinal Astrocytes; Human Retinal Endothelial Cells; Intermittent Hypoxia; Non-Steroidal Anti-Inflammatory Drugs

INTRODUCTION

Retinopathy of Prematurity (ROP) is the leading cause of blindness in extremely low gestational age neonates (ELGANs) requiring supplemental oxygen and mechanical ventilation [1,2]. Although the exact etiology of ROP is unknown, emerging data suggest that ELGANs with chronic lung disease who experience the greatest fluctuations in their PaO₂, or intermittent hypoxia (IH) are at a higher risk for the development of threshold ROP [3–5]. Minimizing repeated episodes of IH significantly decreased the incidence of severe ROP from 12.5% to 2.5% and eliminated the need for laser treatment [6]. A major challenge in the treatment and/or prevention of ROP is the development of safe, “baby-friendly”, and effective pharmacologic interventions that target the aberrant biomolecular pathways in pathologic angiogenesis. Numerous therapies have been implemented and while some exhibited promising short-term benefits, serious long term adverse effects, or “drug disasters” emerged after years of follow-up [7]. Lack of robust preclinical studies; use of off-label and suboptimal formulations; and limited pharmacokinetic/pharmacodynamic/pharmacogenomic and dose determination studies, contribute to these treatment failures and drug disasters [8]. In addition, dosing regimens for ELGANs are still being extrapolated from doses used in adults and older children with adjustments for body weight and/or size [9], or just simply by halving the adult dose [10], without factoring the developmental differences in retinal vasculature, the role of astrocytes during retinal development, the composition of vitreous fluid, and immaturity of drug metabolizing enzymes and transporters, that exist between preterm infants and adults.

Intravitreal administration of anti-vascular endothelial growth factor (VEGF) drugs are effective for adult retinopathy, such as macular degeneration and diabetic retinopathy. However, there are major developmental differences between the preterm neonate and adult vitreous fluid composition and retinal vasculature that may preclude the use of anti-VEGF therapies in neonates, particularly at the doses recommended (half of the adult dose). For example, the human vitreous fluid undergoes age-related liquefaction. It is almost 100% gelatinous at birth and is liquid after 4 years of age [11,12]. Vitreous gel, compared to liquefied vitreous, lowers oxygen tensions in the retina [12], and may increase the mean resident time of drugs. Therefore, the impact of vitreous liquefaction on the distribution and resident time of ocular drugs must be considered when ocular drugs are being used in the preterm neonate. Furthermore, during retinal development, astrocytes are intimately associated with the retinal vasculature. They emerge from the optic disk before the retinal endothelial cells (ECs), form a scaffold, and produce large amounts of VEGF to promote EC

proliferation, migration and vascular patterning [13,14]. Astrocytes ensheath the retinal vessels providing structure and maintenance of blood-retinal barrier (BRB) integrity. Any disturbances in the astrocytic template adversely affect vascular patterning and contribute to the breakdown of the BRB, thus altering the metabolic profile of the tissue [15,16]. The effects of ocular drugs on immature retinal astrocytes and the composition of the immature vitreous fluid, have largely been ignored.

Drug development targeted for the very vulnerable premature newborn infant to prevent severe ROP is fraught with multiple barriers and challenges. The United States Food and Drug Administration (FDA) recently issued legislation such as the Best Pharmaceuticals for Children Act (BPCA) and the Pediatric Research Equity Act (PREA) that provide incentives for testing and developing drugs for use in children. Topical ocular NSAIDs, such as Acuvail (ketorolac) have been previously used for treatment of ROP in ELGANs [17,18]. Our group has recently shown that the use of non-invasive topical ocular non-steroidal anti-inflammatory drugs (NSAIDs) in combination with systemic caffeine citrate results in a significant reduction in the severity of oxygen-induced retinopathy (OIR) in a rat model of IH [19]. Previous studies in preterm infants These findings confirm that arachidonic acid (AA) metabolites play a key role in IH-induced retinopathy, and should be considered as therapeutic targets for treatment and/or prevention of severe ROP.

As part of our ongoing effort to develop “baby-friendly”, effective therapies, at the right doses, for neonates at risk for severe ROP, and given the differences in vitreous composition between preterm neonates and adults, as well as the role of astrocytes in the development of severe ROP, we conducted a series of experiments to test the hypothesis that co-cultures of human retinal endothelial cells (HRECs) and human retinal astrocytes (HRAs) on 3-dimensional (3-D) hydrogel scaffolds is a more representative biomimetic paradigm of the dynamic BRB than 2-D cultures, and should be utilized for preclinical drug discovery and development studies in preterm infants. To test our hypothesis, we evaluated and compared: 1) efficacy of two NSAIDs used in neonatology, ketorolac and ibuprofen, administered alone or co-administered with caffeine; 2) differential responses of mono- and co-cultures of HRECs and HRAs; 3) responses of cells cultured on Algimatrix versus Geltrex biodegradable 3-D hydrogel scaffolds; and 4) effects of hyperoxia (Hx) and intermittent hypoxia (IH), on secretion of AA metabolites.

MATERIAL AND METHODS

Cells

HRECs (ACBRI-181) were purchased from Cell Systems, Inc. (Kirkland, WA, USA) at 80% confluence (1.5×10^6 cells) and acclimatized for 2–3 hours in an incubator at 37°C prior to plating in specialized medium in P75 flasks. Cells were activated with culture boost containing growth factors, antibiotics (Bac-Off), and 5% amphotericin B. Cell media was changed every 2 days and the cells were passaged at 80% confluence. HRAs (1870) were purchased from ScienCell Research Laboratories (Carlsbad, CA, USA) at 5×10^5 cells and acclimatized prior to plating on poly-L-lysine coated P75 flasks in supplemented astrocyte media according to the manufacturer’s protocol. Cell media was changed every 2 days and the cells were passaged at 80% confluence. At confluence, the cells were removed and re-

plated onto 24-well plates. On the day of the experiment, the media was removed and fresh media containing drugs was added. The cells were immediately placed in the various oxygen environments. Media samples were collected at 72 hours post drug treatment. For 2D co-cultures, cells were plated on 24-well transwell inserts, and for 3-D cultures, cells were plated on 24-well plates containing Algimatrix or Geltrex hydrogel scaffolds. The number of cells was determined with TC20 automatic cell counter (BioRad Life Sciences, Hercules, CA).

2-D Co-cultures

Co-cultures of HRECs and HRAs were cultured on Corning transwell inserts (0.4- μ m pore size) pre-coated with ECM attachment factors, in 24-well plates (Corning, Oneonta, NY). For these experiments, both sides of the transwell inserts were used to enable cell-cell contact. The HRAs were seeded first on the abluminal side of the filter at 5×10^4 cells/well and incubated at 37°C in 5% CO₂ to allow the cells to fully attach. At 24 hours post HRA seeding, the HRECs were seeded on the luminal side of the filter under the same conditions for 24 hours. The inserts were then transferred to sterile 24-well plates and incubated for 4 days with media changes every 48 hours. On the day of the experiment, the media was removed and fresh co-culture media containing drugs was added. The cells were immediately placed in the various oxygen environments and media samples were collected at 72 hours post drug treatment.

Biodegradable 3-D Scaffolds

AlgiMatrix is an animal origin-free sponge made from lyophilized alginate gel. The AlgiMatrix 3D culture system was purchased from ThermoFisher Sci (Waltham, MA, USA) in 24-well plates. Prior to plating, cells at 1×10^6 cells/mL were resuspended in cell culture medium, and 10% (v/v) AlgiMatrix firming buffer. The AlgiMatrix sponges were inoculated with 500 μ L of cell suspension. After 5 minutes, an additional 500 μ L media without AlgiMatrix Firming Buffer was added to the sponges and the plates were incubated at 37°C in a humidified atmosphere of 5% CO₂ in air for 4 days until the appearance of spheroids. Media was changed every 2 days. For co-cultures of HRECs and HRAs, the HRAs were seeded first. This is because in the retina, astrocytes emerge first from the optic disk and lay a template for vascular patterning. At 48 hours post HRA seeding, the AlgiMatrix sponges were turned over for seeding the HRECs. Cellular spheres usually form around days 4–7, therefore, drug treatment started on day 4 post HREC seeding, with media changes every 2 days. Geltrex matrix is a basement membrane extract that contains collagen IV, laminin, and other matrix proteins and growth factors and gels in 5–10 minutes above 15°C. Geltrex was purchased from ThermoFisher Sci and prepared according to the manufacturer's protocol. The Geltrex basement membrane was thawed at 4°C overnight. The following day, the growth surface was coated with 400 μ L ice-cold Geltrex matrix and the plates were placed in the incubator at 37°C for 30 minutes prior to cell seeding. For HREC and HRA co-cultures, HRAs were seeded first and HRECs were seeded on top of the HRAs 48 hours later. Drug treatment started occurred on day 4 post HREC seeding. On the day of the experiment, the media was removed and fresh media containing drugs was added. The cells were immediately placed in the various oxygen environments. Media samples were collected at 72 hours post drug treatment.

Experimental Design

Twenty four-well plates were placed in: 1) Nx (5% CO₂/21% O₂); 2) Hx (50% O₂/5% CO₂); or 3) IH (50% O₂ with brief, episodes of 5% O₂/5% CO₂). In each oxygen environment, plates containing HRECs, HRAs, or HREC/HRA co-cultures on either AlgiMatrix or Geltrex biodegradable 3D scaffolds were treated with either: 1) caffeine citrate (10 µg/mL); 2) 10 ng/mL ketorolac (Acuvail, 0.45% ophthalmic solution of 0.4 mg/mL); 3) ibuprofen (10 µg/mL); 4) caffeine+ketorolac; 5) caffeine+ibuprofen; or 6) equivalent volume sterile normal saline (NS) for a total of 324 plates. The caffeine and ibuprofen doses used in this study are based on serum levels in preterm neonates given standard doses [20,21] and the dose of ketorolac was based on vitreous fluid levels [22]. On the day of the experiment, the media was replaced with fresh media containing drug or NS and the cells were randomly assigned to the various oxygen environments. Media was harvested at 72 hours post treatment. Three wells in each group were pooled for a total of 8 samples per group and analyzed for 8-isoPGF_{2α} (biomarker for oxidative stress); the vasoactive mediators and AA metabolites, prostaglandin E (PGE)₂, PGF_{2α}, 6-KetoPGF_{1α} (stable metabolite of prostacyclin, PGI₂), and TxB₂ (stable metabolite of thromboxane A₂, TxA₂). Immunoreactivity of COX isoforms in mono- and co-cultures of HRECs and HRAs on 2D surfaces were also determined.

Hx and Intermittent Hypoxia Profiles

Cells exposed to Hx and IH were placed into specialized dual subchambers (PROOX model 110 oxygen regulator, Biospherix, Redfield, NY, USA) attached to a C42 oxycycler (BioSpherix). The oxycycler supplied O₂, N₂, and CO₂ to the subchambers and the oxygen environment was monitored with oxygen sensors inside the chambers. For the Hx profile, oxygen was set continuously at 50% and remained constant until the end of the experiment. For the IH profile, oxygen was set at 50% for 30 minutes, followed by three 1-minute hypoxia (5% O₂) episodes, each 10 minutes apart, for a total of eight clustered IH episodes/day [23]. This profile consistently produces severe OIR in our rat model [19, 24–26]. The oxygen content in the media was continuously monitored using an oxyvalidator with an oxygen sensor (BioSpherix) inserted directly into the media of a sacrificial well with cells.

8-isoPGF_{2α} Assay

Isoprostanes are prostanoid derivatives that are produced by the non-enzymatic peroxidation of arachidonic acid through reactive oxygen species (ROS). 8-isoprostane, or 8-isoPGF_{2α} is commonly studied and is abundantly generated in vivo during oxidative stress and lipid peroxidation, and is a reliable and proven biomarker for oxidative stress. Levels of 8-isoPGF_{2α} in the media were determined using commercially-available enzyme immunoassay kits purchased from Enzo (Ann Arbor, MI), according to the manufacturer's protocol.

Prostanoid Assays

Prostanoid secretion in the media was measured using commercially available enzyme immunoassay kits purchased from Enzo Life Sciences according to the manufacturer's

protocol (Farmingdale, NY, USA). The prostanoids measured were PGE₂, PGF_{2α}, 6-KetoPGF_{1α}, and TxB₂.

Immunoreactivity Assays

Cells were plated at the same time onto sterile 16-well culture slides (Fisher Scientific, Pittsburgh, PA) and exposed to similar conditions for the 2-D experiments as described above for HRECs, HRAs and HREC/HRA co-cultures. At 24, 48, and 72 hours, the slides were washed, cells were fixed in 4% paraformaldehyde, permeabilized and incubated with COX-1, COX-2 and COX-3 primary antibodies (Santa Cruz Biotechnology, Dallas, TX); and Alexa Fluor fluorescent secondary antibodies (Life Technologies, Grand Island, NY). Cells were imaged at 20X magnification using an Olympus IX73 inverted microscope system and CellSens imaging software (Olympus, Center Valley, PA).

Statistical Analysis

To determine differences among the oxygen (Nx, Hx and IH), cell types (HRECs, HRAs, and HREC+HRA co-cultures), and treatment (caffeine, ketorolac, ibuprofen, caffeine +ketorolac, caffeine+ibuprofen, and saline) groups, two-way ANOVA was used for normally-distributed data and Kruskal-Wallis test for non-normally-distributed data, following Bartlett's test for normality. Post hoc analysis was performed using the Tukey or Student-Newman-Keuls test. To determine differences between the Algimatrix and Geltrex groups, unpaired t-test was used for normally distributed data, and Mann-Whitney-U test for non-normal data following Levene's test for normality. Significance was set at $p < 0.05$ and data are reported as mean \pm SEM. All analyses were two-tailed and performed using SPSS software version 16.0 (SPSS Inc., Chicago, IL) and GraphPad Prism software version 5.02 (GraphPad Inc., San Diego, CA).

RESULTS

Effect on 8-isoPGF_{2α}

The retina is one of the main targets of ROS due to the high content of fatty acids, including AA, leading to lipid peroxidation, a leading cause of retinopathy. 8-iso-PGF_{2α}, which is generally produced independent of COX elicits a potent retinal vasoconstriction by activating the COX pathway. Figure 1 demonstrates the production of 8-iso-PGF_{2α} in 2-D cultures (panels A–C). HRECs cultured on 2-D surfaces secreted higher levels of 8-iso-PGF_{2α} when exposed to IH. Caffeine suppressed 8-iso-PGF_{2α}, but NSAIDs alone and co-administered with caffeine was significantly more effective for reducing 8-iso-PGF_{2α} secretion (Figure 1A). HRAs secreted comparatively lower levels of 8-iso-PGF_{2α} than HRECs but exhibited a similar response pattern, albeit to a much lesser degree (Figure 1B). Co-cultures of HRECs and HRAs resulted in enhanced production of 8-iso-PGF_{2α} in the saline groups, particularly in IH. In the 2-D co-cultures, the inhibitor effect of caffeine and/or NSAIDs on 8-iso-PGF_{2α} was diminished (Figure 1C). Figure 2 represents production of 8-iso-PGF_{2α} from cells cultured on 3-D AlgiMatrix hydrogels (panels A & B), and 3-D Geltrex hydrogels (panels C & D), in HRECs (panels A & C), and HRECs co-cultured with HRAs (panels B & D). HRAs cultured alone on 2D surfaces did not secrete 8-iso-PGF_{2α} in the media. HRECs cultured on AlgiMatrix (Figure 2A) and Geltrex (Figure 2C) secreted

lower 8-iso-PGF_{2α} levels compared to 2D cultures, and the suppressive effect of caffeine and/or NSAIDs was weakened. Similarly, co-cultures on 3-D scaffolds secreted much lower levels of 8-iso-PGF_{2α} than 2-D, suggesting less oxidative stress responses, but the suppressive effects of caffeine and/or NSAIDs was relatively more robust. HRAs cultured alone on 3-D hydrogel scaffolds did not secrete 8-iso-PGF_{2α} into the media.

Effect on PGE₂

PGE₂ has dual opposing effects on endothelial cells. It mediates vasoconstriction when signaling via EP-1 and EP-4 receptor subtypes, and mediates vasodilation through EP-2 and EP-4. PGE₂ is the principle metabolite of the COX-2 isoform which is activated by cytokines and growth factors, and is highly involved in angiogenesis. Figures 3–5 represent the production of PGE₂ by cells cultured on 2-D surfaces (Figure 3, panels A–C), 3-D Algimatrix scaffolds (Figure 4, panels A–C), and 3-D Geltrex scaffolds (Figure 5, panels A–C). Data showed that both HRECs and HRAs produced more PGE₂ when cultured on 2-D surfaces than on 3-D scaffolds suggesting higher induction of the inflammatory COX-2. Moreover, HRECs exposed to IH produced very high levels of PGE₂ (Figures 3A, 4A and 5A). Although caffeine moderately suppressed PGE₂, the effect was not as potent as that of NSAIDs. The response pattern of HRAs cultured on 2-D surfaces was similar to that of HRECs, but the suppressive effect of NSAIDs on PGE₂ secretion by co-cultures was diminished in IH (Figure 3C). When cultured on 3-D scaffolds, the HRECs secretory patterns of PGE₂ and responses to NSAIDs and/or caffeine were similar, but those of the HRAs differed. HRAs cultured on AlgiMatrix 3-D scaffolds produced much higher levels of PGE₂ and the effect of NSAIDs and/or caffeine was less potent (Figure 4B) than those cultured on Geltrex 3-D scaffolds (Figure 5B). Similar response patterns and differences in NSAID potencies were noted for the co-cultures on 3-D scaffolds (Figures 4C and 5C). Overall, 3-D co-cultures elicited stronger responses to treatment.

Effect on PGF_{2α}

ROS generates COX-2-derived PGF_{2α} in oxidative stress, and is a prerequisite for EC dysfunction. PGF_{2α} is a potent vasoconstrictor that increases its own synthesis by increasing the expression of COX-2 through its FP receptor. Figures 6–8 represent the production of PGF_{2α} by cells cultured on 2-D surfaces (Figure 6, panels A–C), 3-D Algimatrix scaffolds (Figure 7, panels A–C), and 3-D Geltrex scaffolds (Figure 8, panels A & B). HRECs and HRAs produce high levels of PGF_{2α} in Hx and IH suggesting a COX-2 effect. There were significant differences in the response patterns among the various 2-D cell cultures. In HRECs, caffeine had some suppressive effects on PGF_{2α}, but ketorolac and co-administration with caffeine exhibited the most suppressive effects (Figure 6A). Surprisingly, the potency of ibuprofen and its co-administration with caffeine, was significantly diminished. Cultures on 3-D scaffolds showed an overall stronger effect of NSAIDs, although the effect was somewhat diminished in HRECs exposed to IH and cultured on Geltrex (Figure 8A) compared to Algimatrix (Figure 7A). HRAs produced much lower levels of PGF_{2α} on AlgiMatrix 3-D scaffolds (Figure 7B), and levels were not detectable in the Geltrex 3-D scaffolds, compared to 2D surfaces, although the potency of NSAIDs were more consistent on 2-D surfaces (Figure 6B). The response patterns of co-

cultures were consistent among the 2-D and 3-D cultures, but the potencies of the NSAIDs were greater in the Geltrex 3-D cultures (Figure 8B).

Effect on 6-ketoPGF_{1α}

The retina and its vasculature predominantly generate PGI₂, rather than PGE₂. PGI₂ counteracts the biological effects of TxA₂ by acting on and desensitizing the TP receptor. It is a platelet de-aggregating factor and potent vasodilator that is induced by COX-2 and involved in angiogenesis. In our experimental conditions, 6-ketoPGF_{1α}, the stable metabolite of PGI₂, was abundantly secreted by HRECs and to a lesser degree, by HRAs, particularly under IH conditions. Figures 9–11 represent the production of 6-ketoPGF_{1α} by cells cultured on 2-D surfaces (Figure 9, panels A–C), 3-D Aligimatrix scaffolds (Figure 10, panels AC), and 3-D Geltrex scaffolds (Figure 11, panels A–C). Data showed that HRAs appeared to enhance the secretion of 6-ketoPGF_{1α} by HRECs in the co-cultures. Monocultures of HRECs on 2-D surfaces were not responsive to ibuprofen and its co-treatment with caffeine (Figure 9A). NSAIDs were more effective for suppressing 6-ketoPGF_{1α} in HRECs cultured on both 3-D scaffolds (Figures 10A and 11A). NSAIDs and/or caffeine equally suppressed 6-ketoPGF_{1α} secreted by HRAs cultured on 2-D surfaces (Figure 9B). Levels of 6-ketoPGF_{1α} were generally higher in the 2-D cultures than 3-D cultures. NSAIDs suppressed 6-ketoPGF_{1α} in both AlgiMatrix (Figure 10C) and Geltrex (Figure 11C) 3-D co-cultures, but the suppressive effect was stronger in the Geltrex cultures.

Effect on TxB₂

TxA₂ is predominantly a COX-1 product. It is a platelet aggregating factor and potent vasoconstrictor with opposing PGI₂ effects. TxA₂ mediates its constrictor actions via TP receptors which are also activated by iso-eicosanoids such as 8-isoPGF_{2α}. Figures 12–14 represent the production of TxB₂ by cells cultured on 2-D surfaces (Figure 12, panels A–C), 3-D Aligimatrix scaffolds (Figure 13, panels A–C), and 3-D Geltrex scaffolds (Figure 14, panels A & B). The data showed that levels of TxB₂, the stable metabolite of TxA₂, was much higher in media from HRECs and HREC+HRA co-cultures on 3-D scaffolds than on 2-D surfaces. The responses of higher TxB₂ levels with ibuprofen and/or caffeine in HRECs cultured on 2-D surfaces mirrored those of PGF_{2α} and 6-ketoPGF_{1α}, suggesting an interaction among those prostanoids (Figure 12A). The responses of TxB₂ were similar in cells cultured on both 3-D scaffolds, although levels were higher in the Geltrex groups (Figure 14). HRAs minimally produced TxB₂ on 2-D (Figure 12B) and Aligimatrix 3-D (Figure 13B) scaffolds, and were not detectable in media from the Geltrex groups. TxB₂ levels and suppressive effect of NSAIDs were highest in co-cultures Geltrex 3-D scaffolds (Figure 14B) compared to 2-D (Figure 12C) and AlgiMatrix 3-D scaffolds (Figure 13C). In those groups, cells cultured under IH conditions appeared to be resistant to NSAID treatment.

Effect on COX-1

HRECs moderately expressed COX-1 (green) under control conditions (Figure 15A) and the expression is increased in IH (Figure 15M). Caffeine suppressed COX-1 in Nx (Figure 15B) and Hx (Figure 15H) conditions, but the effect was diminished in IH (Figure 15N). Ketorolac suppressed COX-1 in all conditions (Figures 15C, 15I and 15O). Ibuprofen

suppressed COX-1 in Nx (Figure 15D), but the effect was diminished in Hx (Figure 15J) and IH (Figure 15P). Caffeine+ketorolac did not appreciably suppress COX-1 (Figures 15E, 15K, and 15Q). Caffeine+ibuprofen was most effective in Nx (Figures 15F) and IH (Figures 15R). Figure 16 shows COX-1 immunoreactivity in HRAs. COX-1 (red) was suppressed in HRAs exposed to Hx (Figure 16G) and in the caffeine (Figure 16H), ketorolac (Figure 16I), ibuprofen (Figure 16J), and caffeine+ketorolac (Figure 16K) groups exposed to Hx.

Effect on COX-2

COX-2 expression in HRECs (green) was increased in Hx (Figure 17G) and more robustly in IH (Figure 17M). Caffeine obliterated COX-2 expression in Nx (Figure 17B) and Hx (Figure 17H), but the effect was diminished in IH (Figure 17N). Ketorolac did not appreciably affect COX-2 in Nx (Figure 17C) or Hx (Figure 17I) but decreased it in IH (Figure 17O), compared to saline treatment in IH. Ibuprofen effectively diminished COX-2 in all oxygen conditions (Figures 17D, 17J, and 17P). Caffeine+ketorolac reduced COX-2 in Nx (Figure 17E), and to a lesser degree in Hx (Figure 17K) and IH (Figure 17Q), but the reactivity was reduced compared to saline. Similar responses were noted for caffeine +ibuprofen (Figure 17F, 17L, and 17R). COX-2 immunoreactivity (red) is presented in Figure 18. The responses of NSAID treatment in HRAs on COX-2 immunoreactivity reflected those of COX-1.

DISCUSSION

The standard models used in the drug development process involve 2-D in-vitro models. Drug screening based on simple 2-D culture systems can predict drug toxicity, but remains limited. Emerging evidence suggest that 3-D cultures are more physiologically relevant, and representative of in-vivo cell behavior such as adhesion, growth and differentiation (biomimicry), reproducing the cell-cell and cell-extracellular matrix (ECM) interactions, compared to cells cultured in a 2-D environment [27,28]. Because the premature vitreous fluid composition is almost 100% gelatinous compared to the more liquefied vitreous fluid of adults, and considering the role of astrocytes in retinal development and BRB integrity [13–16], we evaluated two 3-D biodegradable hydrogel scaffolds, AlgiMatrix (algae-based) and Geltrex (animal-based) and compared the responses of HREC and HRA mono- and co-cultures (replicating the BRB). In addition, as a follow-up to our recent findings of a therapeutic potential for ocular NSAIDs and systemic caffeine [19], we compared the effects of ketorolac or ibuprofen alone, or co-administered with caffeine, on AA metabolites. The major findings of this study are: 1) Cells cultured on 3-D scaffolds exhibited less oxidative stress responses; 2) HRAs enhance and promote the responses of HRECs in IH; 3) PGE₂ and PGI₂ were the predominant prostanoids produced by HRECs in IH, concurrent with robust immunoreactivity of COX-2. NSAIDs suppression of PGE₂ and PGI₂ secretion were more potent in the co-cultures than mono-cultures; 4) Both NSAIDs significantly suppressed prostanoid secretion, but the effects were more potent in the Geltrex 3-D cultures. Astrocyte mono-cultures responded more favorably to AlgiMatrix, but when co-cultured with HRECs, the responses favored Geltrex; and 5) Distinct similarities existed among the PGF_{2α}, 6-ketoPGF_{1α}, TxB₂ responses to ibuprofen in HRECs cultured on 2-D surfaces, indicating interaction among these prostanoids. Collectively, these findings provide evidence that PGE₂

and PGI₂ may be potential therapeutic targets, possibly via COX-2 inhibition, for IH-induced retinopathy. Furthermore, the use of HRA/HREC co-cultures on Geltrex or similar 3-D biodegradable hydrogel scaffolds, may be a more appropriate biomimetic paradigm for ocular drug discovery and development, and drug screening studies.

AA, a 20-carbon polyunsaturated fatty acid abundant in cell membrane phospholipids, is released in response to numerous stimuli, into the cytoplasm by the action of phospholipase A₂. Free AA is subjected to a number of reactions to form the unstable prostaglandin endoperoxide (PGH₂) [29,30], which serves as a substrate for a number of cell-specific isomerases and synthases to produce biologically active prostaglandins (PGs), prostacyclin (PGI₂), and thromboxane (TxA₂), also known as prostanoids [31]. Prostanoids are vasoactive and proinflammatory mediators that play a key role in regulation of blood flow and vasomotor tone in the retina [32]. In oxidative stress, free AA can also accumulate and undergo uncontrolled oxidative metabolism by both enzymatic and non-enzymatic processes, known as the “AA cascade” [32]. The AA cascade amplifies the production of reactive oxygen species (ROS), and subsequently causes oxidative damage to lipids, proteins, and nucleic acids [33]. AA itself is also subject to free radical attack, leading to formation of prostaglandin isomers known as isoeicosanoids or isoprostanes, within the cell membrane phospholipid [34]. Isoprostanes are potent vasoconstrictors and in high enough concentrations can result in vasoconstriction, and platelet aggregation, via action on PG (TxA₂, and PGF_{2α}) receptors, namely, TP and FP, respectively. Of the isoprostanes, the most commonly studied is 8-isoPGF_{2α}, also known as 8-isoprostane, which is considered the most reliable biomarker for oxidative stress [35]. In the retina, fatty acids accumulate rapidly during the later stages of gestation and early postnatal life [36]. Thus, the retina contains a high concentration of fatty acids, including AA, making it susceptible to the AA cascade and ROS attack. Therefore, curtailing the AA cascade may represent one mechanism for the benefits of NSAIDs in OIR [19]. In the present study, both HRECs and HRAs responded to Hx and IH by secreting high levels of 8-isoPGF_{2α}, with the highest levels produced in IH. Caffeine suppressed 8-isoPGF_{2α}, but not as effectively as NSAIDs. This confirms the antioxidant properties of ketorolac and to a lesser degree, caffeine, and strongly suggests that 8-isoPGF_{2α} may also be generated via the COX enzymatic pathway under certain conditions. Astrocytes do not appear to secrete 8-isoPGF_{2α} in response to oxidative stress, at least when cultured on 3-D biodegradable scaffolds, but when co-cultured with HRECs, can induce even higher secretion by HRECs. This enhanced effect is likely due to IH-activated gliosis, which is known to induce ROS [37]. While ocular drugs that target retinal ECs may be effective, the role of astrocytes in oxidative stress and ocular diseases must also be considered.

COX exists in 2 isoforms (COX-1 and COX-2) that regulate the production of prostanoids. COX-1 is constitutively expressed at high levels in cells and tissues and is the major isoform expressed in healthy tissue. It generates prostanoids for many functions including vasomotor tone and platelet aggregation. COX-2 is present at a basal level in certain tissues but its expression is induced in response to inflammatory and mitogenic stimuli [38]. COX-2 stimulates angiogenesis by promoting the production of TxA₂, PGE₂, and PGI₂, which are direct stimulants of endothelial cells [39–41]. COX-2 correlates with VEGF expression [42] and vascular function, and may contribute to retinal angiogenesis [43]. We, and others, have

shown that COX inhibition reduces the severity of OIR and ROP [44–48], demonstrating that the COX/ROS pathways are inextricably linked and highly involved in the development of aberrant angiogenesis. The influence of COX in the development of ROP support the need for further drug development/screening studies. Our data showed that PGE₂ and PGF_{2α} (produced predominantly by HRECs), as well as COX-2, were higher in the IH group, and the response patterns were similar in both 3-D platforms. However, there was a much higher response of the co-cultures in Geltrex, further indicating that cross-talk between HREC and HRA produces amplified responses that may recapitulate that of the BRB. Both NSAIDs successfully decreased PGE₂ although ibuprofen alone or co-administered with caffeine was more effective. The action of prostanoids can cause vasodilatation, breakdown of BRB, and subsequently hemorrhage. Our study showed that PGI₂ was the predominant prostanoid produced by HRECs, with the highest levels secreted during IH. While HRAs minimally secrete PGI₂ relative to HRECs, the responses to IH reflected those of the HRECs. PGI₂ is one of the most important prostanoids that regulates vascular homeostasis, is abundant in the retina, and is responsible for relaxation of the retinal microvasculature [49]. ECs and endothelial progenitor cells are the major sources of PGI₂ [50], generated preferentially by COX-2 [51]. Studies have shown that PGI₂ is decreased during the ischemic phase of OIR, but may increase during the proliferative phase [52], possibly in response to resumption of oxygen to elevate blood flow. The finding of higher PGI₂ in IH suggests induction of COX-2, likely because of inflammation, ROS accumulation, and higher VEGF levels, indicating that the use of NSAIDs with a higher specificity for PGI₂, may have potential therapeutic benefits in the setting of IH-induced retinopathy. Of the two NSAIDs examined in this study, ketorolac alone and co-administered with caffeine, exhibited a stronger suppressive effect on PGI₂, in HRECs cultured on 2-D surfaces, but showed stronger effects in HRAs and co-cultures, as well as in the Geltrex 3-D groups. These findings demonstrate variability in drug responses between mono- and co-cultures and between 2-D and 3-D platforms. Thus, limiting drug development/screening studies to monocultures or 2-D platforms may lead to treatment failures. More dose-response studies involving other NSAIDs are needed to identify the most effective treatment.

ECM composition plays a key role in EC intrusive and migration behaviors. Cells interact with their ECM and change their microenvironment in response to drugs. While there are no in-vitro models that completely exhibits biomimicry with all the complexities of the in-vivo environment, recent advancements involving 3-D scaffolds and co-culture systems have led to a clearer understanding of the biomolecular processes associated with cellular responses to drugs. In 3-D cultures, cells can exhibit phenotypes, respond to stimuli, and utilize their artificial scaffolds as support matrices consistent with the in-vivo ECM. In the current study, we used two hydrogels, AlgMatrix, an animal-free, highly porous, non-toxic, biodegradable bioscaffold sponge made from lyophilized alginate gel; and Geltrex, a virus-free soluble form of reduced growth factor basement membrane matrix extracted from murine Engelbreth-Holm-Swarm tumors, comprising laminin, collagen IV, entactin, and heparin sulfate proteoglycans. Hydrogel matrices, like AlgMatrix and Geltrex, are water soluble polymers that are appealing for ocular applications due to their high water content, similar to the vitreous fluid. An advantage of hydrogels is that they can protect drugs, enhance mean resident time, and sustained drug delivery [53]. There are many problems associated with

ocular drug development in neonates, including immaturity of the BRB, variability in pharmacology, and lack of dose-dependent studies to define appropriate dosing regimens. Notwithstanding, well-designed, multi-center clinical drug trials in critically ill micropremies, at the beginning of their lives and fighting heroically to survive, may be potentially shortened and be more successful with significantly less adverse outcomes, if potential therapies are subjected to robust, rigorous, and focused preclinical research efforts that clearly identify the most effective and safe targets in a timely manner. Sadly, too many treatment strategies are implemented in this vulnerable population without adequate preclinical investigation, using appropriate models, and are doomed to failure. The current findings show that co-cultures of HRECs and HRAs on 3-D biodegradable scaffolds can and should be utilized for drug development/screening biomimetic paradigms to recapitulate the functionality and drug responses of the dynamic in-vivo environment of the BRB. Co-cultures of HRECs and HRAs on 3-D scaffolds are powerful biomimetic models for preclinical drug discovery and development, and should be utilized during the first few stages of new drug development/screening for target identification, drug dosing optimization, and reduction in drug toxicity and treatment failures during the later phase II/III trials. Further dose-response studies involving other ocular NSAIDs and/or selective COX-2 inhibitors are needed to identify the best pharmacologic profiles and ocular delivery methods that are safe, effective, and baby-friendly, for the prevention of ROP.

Acknowledgments

Financial support: This work was made possible through the Eunice Kennedy Shriver National Institute of Child Health & Human Development Grant #1U54HD071594.

Abbreviations

3-D	3-dimensional
AA	arachidonic Acid
ANOVA	analysis of variance
BPCA	best pharmaceuticals children's act
BRB	blood retina barrier
COX	cyclooxygenase
ECM	extracellular matrix
ELGANs	extremely low gestational age neonates
FDA	food and drug administration
HRA	human retinal astrocytes
Hx	hyperoxia
IGF-I	insulin-like growth factor-I

IH	intermittent hypoxia
NSAIDs	non-steroidal anti-inflammatory drugs
Nx	normoxia
OIR	oxygen-induced retinopathy
PGs	prostaglandins
PREA	pediatric research equity act
ROP	retinopathy of prematurity
ROS	reactive oxygen species
sVEGFR-1	soluble vascular endothelial growth factor receptor-1
VEGF	vascular endothelial growth factor

References

1. Gilbert C, Fielder A, Gordillo L, et al. Characteristics of infants with severe retinopathy of prematurity in countries with low, moderate, and high levels of development: implications for screening programs. *Pediatrics*. 2005; 115:e518–e525. [PubMed: 15805336]
2. Kong L, Fry M, Al-Samarraie M, Gilbert C, Steinkuller PG. An update on progress and the changing epidemiology of causes of childhood blindness worldwide. *J AAPOS*. 2012; 16:501–507. [PubMed: 23237744]
3. York JR, Landers S, Kirby RS, Arbogast PG, Penn JS. Arterial oxygen fluctuation and retinopathy of prematurity in very-low-birth-weight infants. *J Perinatol*. 2004; 24:82–87. [PubMed: 14762452]
4. Di Fiore JM, Bloom JN, Orge F, et al. A higher incidence of intermittent hypoxemic episodes is associated with severe retinopathy of prematurity. *J Pediatr*. 2010; 157:69–73. [PubMed: 20304417]
5. Di Fiore JM, Kaffashi F, Loparo K, et al. The relationship between patterns of intermittent hypoxia and retinopathy of prematurity in preterm infants. *Pediatr Res*. 2012; 72:606–612. [PubMed: 23037873]
6. Chow LC, Wright KW, Sola A, et al. Can changes in clinical practice decrease the incidence of severe retinopathy of prematurity in very low birth weight infants? *Pediatrics*. 2003; 111:339–345. [PubMed: 12563061]
7. Beharry KD, Valencia GB, Lazzaro DR, Aranda JV. Pharmacologic interventions for the prevention and treatment of retinopathy of prematurity. *Semin Perinatol*. 2016; 40:189–202. [PubMed: 26831641]
8. de Souza AS Jr, Dos Santos DB, Rey LC, Medeiros MG, Vieira MG, Coelho HL. Off-label use and harmful potential of drugs in a NICU in Brazil: A descriptive study. *BMC Pediatr*. 2016; 16:13. [PubMed: 26795213]
9. Allegaert K, van den Anker JJ. Neonatal drug therapy: The first frontier of therapeutics for children. *Clin Pharmacol Ther*. 2015; 98:288–97. [PubMed: 26095519]
10. Mintz-Hittner HA, Kennedy KA, Chuang AZ. BEAT-ROP Cooperative Group. Efficacy of intravitreal bevacizumab for stage 3+ retinopathy of prematurity. *N Engl J Med*. 2011; 364:603–615. [PubMed: 21323540]
11. Le Goff MM, Bishop PN. Adult vitreous structure and postnatal changes. *Eye*. 2008; 22:1214–1222. [PubMed: 18309340]
12. Balazs, EA., Denlinger, JL. Ageing changes in the vitreous. In: Dismukes, K., Sekular, R., editors. *Ageing and human visual function*. Alan R Liss, Inc; New York: 1982. p. 45-57.

13. Dorrell MI, Aguilar E, Friedlander MM. Retinal vascular development is mediated by endothelial filopodia, a preexisting astrocyte template and specific R-cadherin adhesion. *Invest Ophthalmol Vis Sci.* 2002; 43:3500–3510. [PubMed: 12407162]
14. Chan-Ling T, McLeod DS, Hughes S, et al. Astrocyte-endothelial cell relationships during human retinal development. *Invest Ophthalmol Vis Sci.* 2004; 45:2020–2032. [PubMed: 15161871]
15. Chan-Ling T, Stone J. Degeneration of astrocytes in feline retinopathy of prematurity causes failure of the blood-retinal barrier. *Invest Ophthalmol Vis Sci.* 1992; 33:2148–59. [PubMed: 1607225]
16. Weidemann A, Krohne TU, Aguilar E, et al. Astrocyte hypoxic response is essential for pathological but not developmental angiogenesis of the retina. *Glia.* 2010; 58:1177–85. [PubMed: 20544853]
17. Avila-Vazquez M, Maffrand R, Sosa M, et al. Treatment of retinopathy of prematurity with topical ketorolac tromethamine: a preliminary study. *BMC Pediatr.* 2004; 7:415.
18. Giannantonio C, Purcaro V, Cota F, et al. Effectiveness of ketorolac tromethamine in prevention of severe retinopathy of prematurity. *J Pediatr Ophthalmol Strabismus.* 2011; 48:247–51. [PubMed: 20873697]
19. Aranda JV, Cai CL, Ahmad T, et al. Pharmacologic synergism of ocular ketorolac and systemic caffeine citrate in rat oxygen-induced retinopathy. *Pediatr Res.* 2016; 80:554–65. [PubMed: 27438224]
20. Aranda JV, Collinge JM, Zinman R, Watters G. Maturation of caffeine elimination in infancy. *Arch Dis Child.* 1979; 54:946–9. [PubMed: 533298]
21. Van Overmeire B, Touw D, Schepens PJ, Kearns GL, van den Anker JN. Ibuprofen pharmacokinetics in preterm infants with patent ductus arteriosus. *Clin Pharmacol Ther.* 2001; 70:336–43. [PubMed: 11673749]
22. Schoenberger SD, Kim SJ, Sheng J, Calcutt MW. Reduction of vitreous prostaglandin E2 levels after topical administration of ketorolac 0.45%. *JAMA Ophthalmol.* 2014; 132:150–4. [PubMed: 24264034]
23. Quan M, Cai CL, Valencia GB, Aranda JV, Beharry KD. MnTBAP or catalase is more protective against oxidative stress in human retinal endothelial cells exposed to intermittent hypoxia than their co-administration (EUK-134). *ROS J.* 2017; 3:47–65.
24. Tu C, Beharry KD, Shen X, et al. Proteomic profiling of the retinas in a neonatal rat model of oxygen-induced retinopathy with a reproducible ion-current-based MS1 approach. *J Proteome Res.* 2015; 14:2109–20. [PubMed: 25780855]
25. Beharry KD, Cai CL, Sharma P, et al. Hydrogen peroxide accumulation in the choroid during intermittent hypoxia increases risk of severe oxygen-induced retinopathy in neonatal rats. *Invest Ophthalmol Vis Sci.* 2013; 54:7644–7657. [PubMed: 24168990]
26. Tan JJ, Cai CL, Shrier EM, McNally L, Lazzaro DR, Aranda JV, Beharry KD. Ocular Adverse Effects of Intravitreal Bevacizumab Are Potentiated by Intermittent Hypoxia in a Rat Model of Oxygen-Induced Retinopathy. *J Ophthalmol.* 2017:4353129. [PubMed: 28770109]
27. Baker BM, Chen CS. Deconstructing the third dimension: how 3D culture microenvironments alter cellular cues. *J Cell Sci.* 2013; 125:3015–24.
28. Birgersdotter A, Sandberg R, Ernberg I. Gene expression perturbation in vitro--a growing case for three-dimensional (3D) culture systems. *Semin Cancer Biol.* 2005; 15:405–12. [PubMed: 16055341]
29. FitzGerald GA, Patrono C. The coxibs, selective inhibitors of cyclooxygenase-2. *N Engl J Med.* 2001; 345:433–42. [PubMed: 11496855]
30. Rao PNP, Knaus EE. Evolution of Nonsteroidal Anti-Inflammatory Drugs (NSAIDs): Cyclooxygenase (COX) Inhibition and Beyond. *J Pharm Pharmaceut Sci.* 2008; 11:81s–110s.
31. Funk RH. Blood supply of the retina. *Ophthalmic Res.* 1997; 29:320–5. [PubMed: 9323723]
32. Morrow JD, Hill KE, Burk RF, Nammour TM, Badr KF, Roberts LJ 2nd. Formation of unique biologically active prostaglandins in vivo by a non-cyclooxygenase free radical catalyzed mechanism. *Adv Prostaglandin Thromboxane Leukot Res.* 1991; 21A:125–8. [PubMed: 1847759]
33. Morrow JD, Hill KE, Burk RF, Nammour TM, Badr KF, Roberts LJ 2nd. A series of prostaglandin F2-like compounds are produced in vivo in humans by a non-cyclooxygenase, free radical-catalyzed mechanism. *Proc Natl Acad Sci USA.* 1990; 87:9383–7. [PubMed: 2123555]

34. Morrow JD. The isoprostanes - unique products of arachidonate peroxidation: their role as mediators of oxidant stress. *Curr Pharm Res.* 2006; 12:895–902.
35. Milne GL, Morrow JD. Isoprostanes and related compounds: update 2006. *Antioxid Redox Signal.* 2006; 8:1379–84. [PubMed: 16910785]
36. Martinez M. Tissue levels of polyunsaturated fatty acids during early human development. *J Pediatr.* 1992; 120:129–138. [PubMed: 1731010]
37. Sheng WS, Hu S, Feng A, Rock RB. Reactive oxygen species from human astrocytes induced functional impairment and oxidative damage. *Neurochem Res.* 2013; 38:2148–59. [PubMed: 23918204]
38. Smith WL, DeWitt DL, Garavito RM. Cyclooxygenases: structural, cellular, and molecular biology. *Annu Rev Biochem.* 2000; 69:145–82. [PubMed: 10966456]
39. Daniel TO, Liu H, Morrow JD, Crews BC, Marnett LJ. Thromboxane A2 is a mediator of cyclooxygenase-2 dependent endothelial migration and angiogenesis. *Cancer Res.* 1999; 59:4574–7. [PubMed: 10493510]
40. Inoue H, Takamori M, Shimoyama Y, Ishibashi H, Yamamoto S, Koshihara Y. Regulation by PGE2 of the production of interleukin-6, macrophage colony stimulating factor, and vascular endothelial growth factor in human synovial fibroblasts. *Br J Pharmacol.* 2002; 136:287–95. [PubMed: 12010778]
41. Murohara T, Horowitz JR, Silver M, et al. Vascular endothelial growth factor/vascular permeability factor enhances vascular permeability via nitric oxide and prostacycline. *Circulation.* 1998; 97:99–107. [PubMed: 9443437]
42. Gately S. The contributions of cyclooxygenase-2 to tumor angiogenesis. *Cancer Metastasis Rev.* 2000; 19:19–27. [PubMed: 11191059]
43. Leahy KM, Ornberg RL, Wang Y, et al. Cyclooxygenase-2 inhibition by celecoxib reduces proliferation and induces apoptosis in angiogenic endothelial cells in vivo. *Cancer Res.* 2002; 62:625–631. [PubMed: 11830509]
44. Ozaki NK, Beharry KD, Nishihara KC, et al. Regulation of retinal vascular endothelial growth factor and receptors in rabbits exposed to hyperoxia. *Invest Ophthalmol Vis Sci.* 2002; 43:1546–1557. [PubMed: 11980873]
45. Chemtob S, Beharry K, Rex J, Chatterjee T, Varma DR, Aranda JV. Ibuprofen enhances retinal and choroidal blood flow autoregulation in newborn piglets. *Invest Ophthalmol Vis Sci.* 1991; 32:1799–1807. [PubMed: 2032803]
46. Hammerman C. Indomethacin and retinopathy of prematurity: The hidden paradox. *J Pediatr.* 2008; 153:587–588.
47. Sharma J, Barr SM, Geng Y, Yun Y, Higgins RD. Ibuprofen improves oxygen-induced retinopathy in a mouse model. *Curr Eye Res.* 2003; 27:309–14. [PubMed: 14562167]
48. Takahashi K, Saishin Y, Mori K, et al. Topical nepafenac inhibits ocular neovascularization. *Invest Ophthalmol Vis Sci.* 2003; 44:409–415. [PubMed: 12506103]
49. Burnette JO, White RE. PGI2 opens potassium channels in retinal pericytes by cyclic AMP-stimulated, cross-activation of PKG. *Exp Eye Res.* 2006; 83:1359–65. [PubMed: 16959250]
50. Kawabe J, Ushikubi F, Hasebe N. Prostacyclin in vascular diseases. *Circ J.* 2010; 74:836–843. [PubMed: 20424334]
51. McAdam BF, Catella-Lawson F, Mardini IA, Kapoor S, Lawson JA, FitzGerald GA. Systemic biosynthesis of prostacyclin by cyclooxygenase (COX)-2: the human pharmacology of a selective inhibitor of COX-2. *Proc Natl Acad Sci USA.* 1999; 96:272–7. [PubMed: 9874808]
52. Stuart MJ, Phelps DL, Setty BN. Changes in oxygen tension and effects on cyclooxygenase metabolites: II. Decrease of retinal prostacyclin in kittens exposed to hyperoxia. *Pediatrics.* 1988; 82:36772.
53. Garg T, Singh O, Arora S, Murthy R. Scaffold: a novel carrier for cell and drug delivery. *Crit Rev Ther Drug Carrier Syst.* 2012; 29:1–63. [PubMed: 22356721]

Highlights

- Cells cultured on 3-D scaffolds tolerated IH more efficiently than 2-D cultures.
- PGE₂ and PGI₂ were the predominant prostanoids produced in response to IH.
- HRAs enhanced the responses of HRECs to drugs and changes in oxygen.

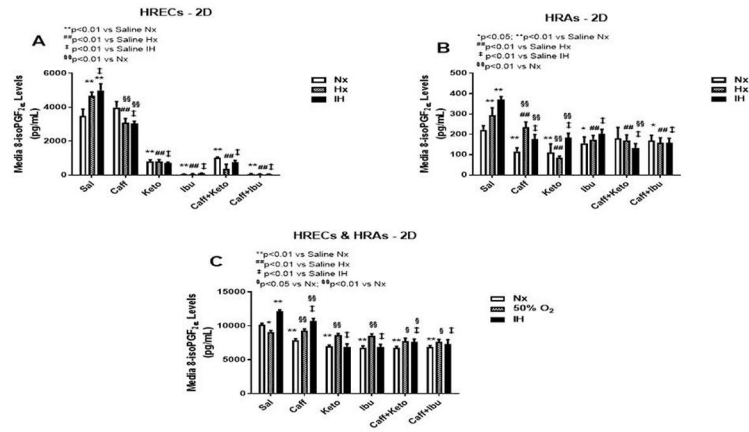


Figure 1. 8-iso-PGF_{2α} levels in media from cells cultured on 2-D surfaces. Panel A represents data from HRECs, panel B from HRAs and panel C from co-cultures of HRECs+HRAs. Data are presented as mean±SEM (n=8 samples/groups). Comparison to saline Nx is represented by *p<0.05; **p<0.01; comparison to saline Hx is represented by #p<0.05; ##p<0.01; comparison to saline IH is represented by †p<0.05; ‡p<0.01; and comparison among the treated groups is represented by §p<0.05; §§p<0.01.

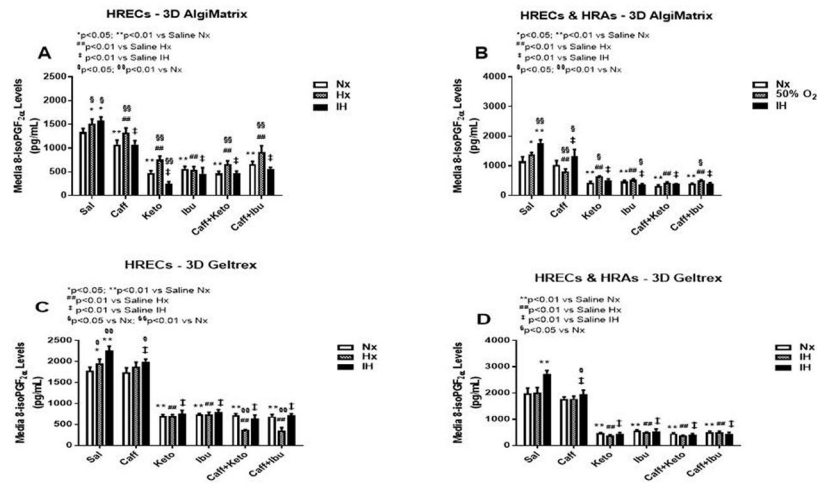


Figure 2. 8-iso-PGF_{2α} levels in media from 3-D Alginate Matrix biodegradable hydrogel scaffolds (panels A & B), and 3-D Geltrex biodegradable hydrogel scaffolds (panels C & D) in HRECs (panels A and C and HREC+HRA co-cultures (panels B & D). Data are presented as mean ±SEM (n=8 samples/groups). Data are presented as mean±SEM (n=8 samples/groups). Comparison to saline Nx is represented by *p<0.05; **p<0.01; comparison to saline Hx is represented by #p<0.05; ##p<0.01; comparison to saline IH is represented by †p<0.05; ††p<0.01; and comparison among the treated groups is represented by §p<0.05; §§p<0.01.

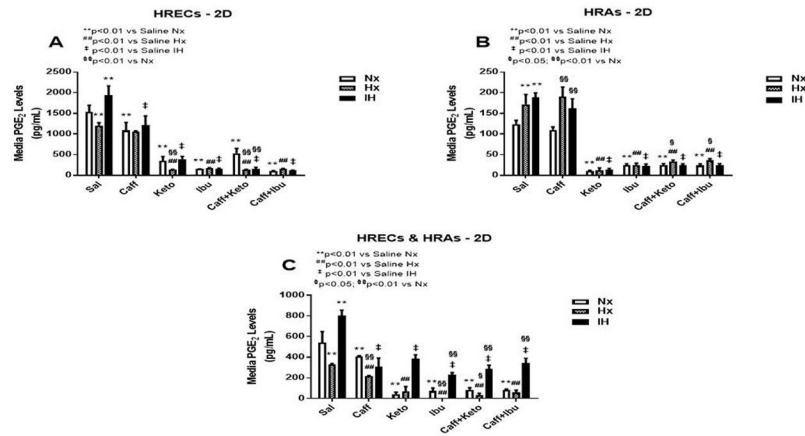


Figure 3.

PGE₂ levels in media from cells cultured on 2-D surfaces. Panel A represents data from HRECs, panel B from HRAs and panel C from co-cultures of HRECs+HRAs. Data are presented as mean±SEM (n=8 samples/groups). Comparison to saline Nx is represented by *p<0.05; **p<0.01; comparison to saline Hx is represented by #p<0.05; ##p<0.01; comparison to saline IH is represented by †p<0.05; ‡p<0.01; and comparison among the treated groups is represented by §p<0.05; §§p<0.01.

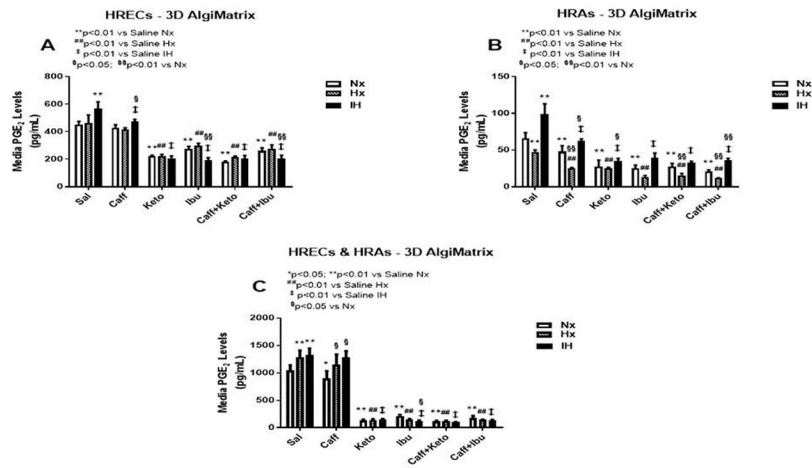


Figure 4. PGE₂ levels in media from 3-D Alginate biodegradable hydrogel scaffolds. Panel A represents data from HRECs, panel B from HRAs and panel C from co-cultures of HRECs +HRAs. Data are presented as mean±SEM (n=8 samples/groups). Data are presented as mean±SEM (n=8 samples/groups). Comparison to saline Nx is represented by *p<0.05; **p<0.01; comparison to saline Hx is represented by #p<0.05; ##p<0.01; comparison to saline IH is represented by †p<0.05; ††p<0.01; and comparison among the treated groups is represented by ‡p<0.05; §§p<0.01.

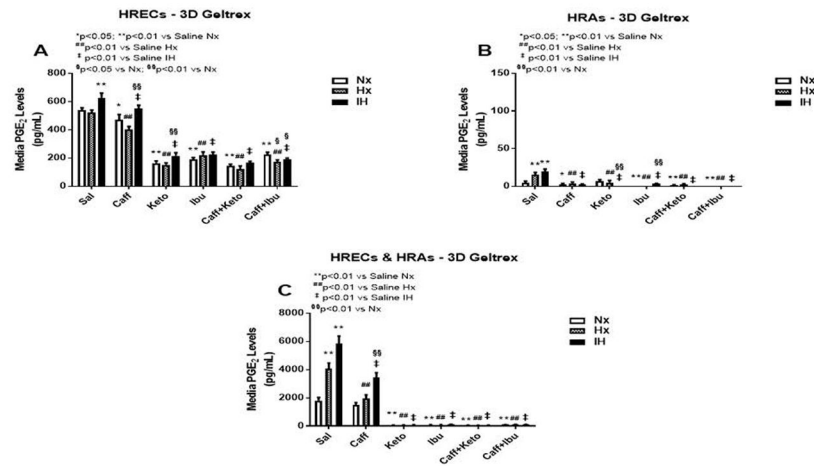


Figure 5. PGE₂ levels in media from 3-D Geltrex biodegradable hydrogel scaffolds. Panel A represents data from HRECs, panel B from HRAs and panel C from co-cultures of HRECs +HRAs. Data are presented as mean±SEM (n=8 samples/groups). Data are presented as mean±SEM (n=8 samples/groups). Comparison to saline Nx is represented by *p<0.05; **p<0.01; comparison to saline Hx is represented by #p<0.05; ##p<0.01; comparison to saline IH is represented by †p<0.05; ††p<0.01; and comparison among the treated groups is represented by §p<0.05; §§p<0.01.

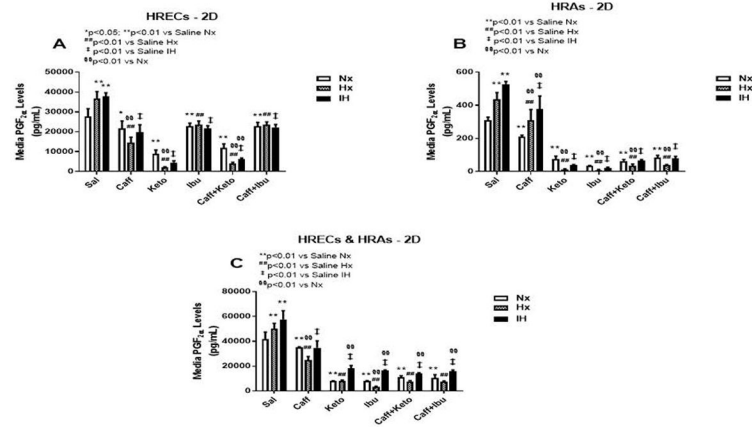
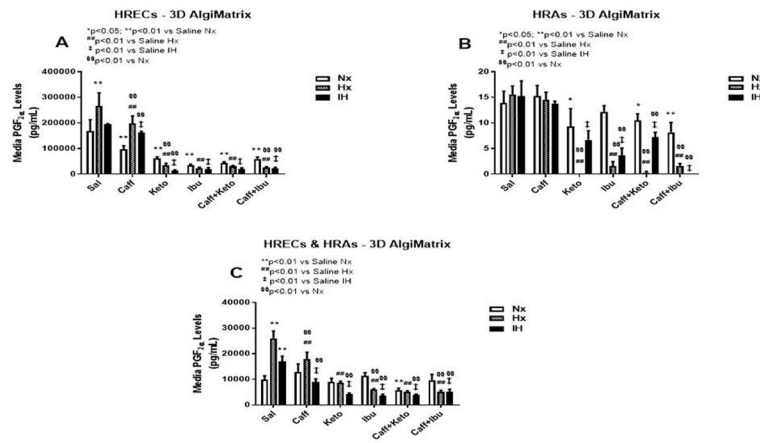


Figure 6.

PGF_{2α} levels in media from cells cultured on 2-D surfaces. Panel A represents data from HRECs, panel B from HRAs and panel C from co-cultures of HRECs+HRAs. Data are presented as mean±SEM (n=8 samples/groups). Comparison to saline Nx is represented by *p<0.05; **p<0.01; comparison to saline Hx is represented by #p<0.05; ##p<0.01; comparison to saline IH is represented by †p<0.05; ††p<0.01; and comparison among the treated groups is represented by §p<0.05; §§p<0.01.

**Figure 7.**

PGF_{2α} levels in media from 3-D Alginate Matrix biodegradable hydrogel scaffolds. Panel A represents data from HRECs, panel B from HRAs and panel C from co-cultures of HRECs +HRAs. Data are presented as mean±SEM (n=8 samples/groups). Data are presented as mean±SEM (n=8 samples/groups). Comparison to saline Nx is represented by *p<0.05; **p<0.01; comparison to saline Hx is represented by #p<0.05; ##p<0.01; comparison to saline IH is represented by †p<0.05; ††p<0.01; and comparison among the treated groups is represented by §p<0.05; §§p<0.01.

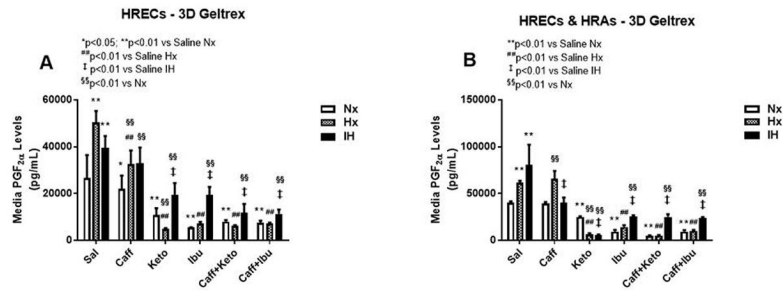
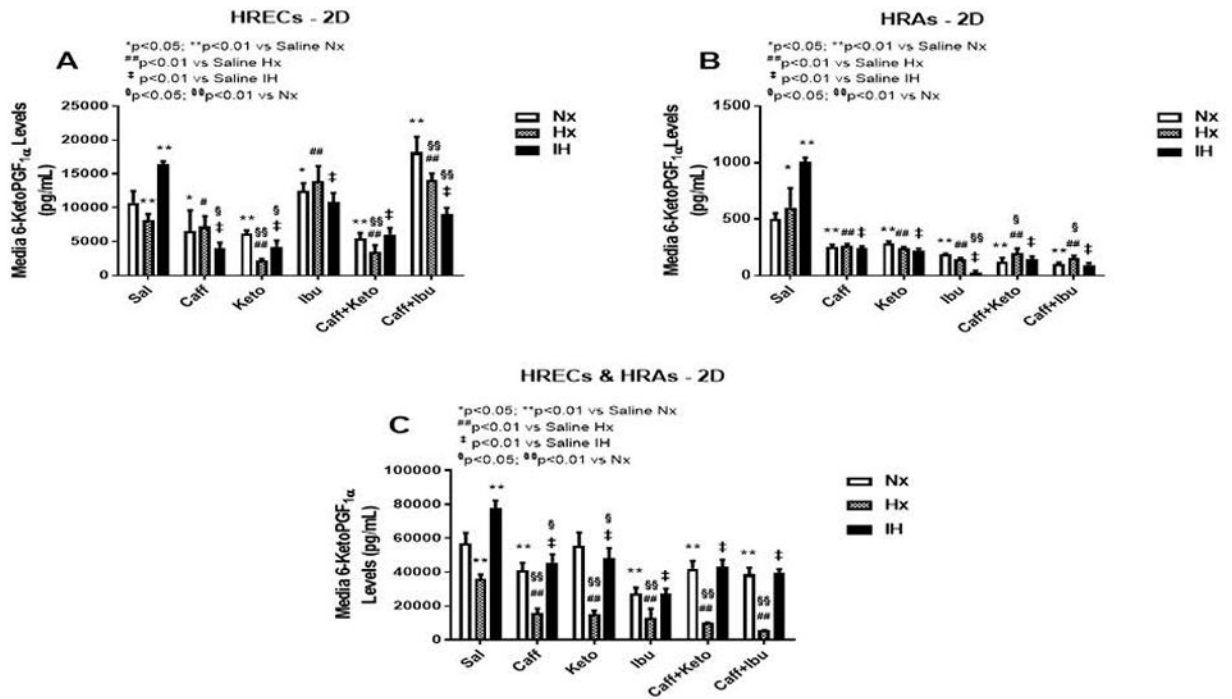


Figure 8. PGF_{2α} levels in media from 3-D Geltrex biodegradable hydrogel scaffolds. Panel A represents data from HRECs, and panel B from co-cultures of HRECs+HRAs. Data are presented as mean±SEM (n=8 samples/groups). Data are presented as mean±SEM (n=8 samples/groups). Comparison to saline Nx is represented by *p<0.05; **p<0.01; comparison to saline Hx is represented by #p<0.05; ##p<0.01; comparison to saline IH is represented by †p<0.05; ‡p<0.01; and comparison among the treated groups is represented by §p<0.05; §§p<0.01.

**Figure 9.**

6-ketoPGF_{1α} levels in media from cells cultured on 2-D surfaces. Panel A represents data from HRECs, panel B from HRAs and panel C from co-cultures of HRECs+HRAs. Data are presented as mean±SEM (n=8 samples/groups). Comparison to saline Nx is represented by *p<0.05; **p<0.01; comparison to saline Hx is represented by #p<0.05; ##p<0.01; comparison to saline IH is represented by †p<0.05; ‡p<0.01; and comparison among the treated groups is represented by §p<0.05; §§p<0.01.

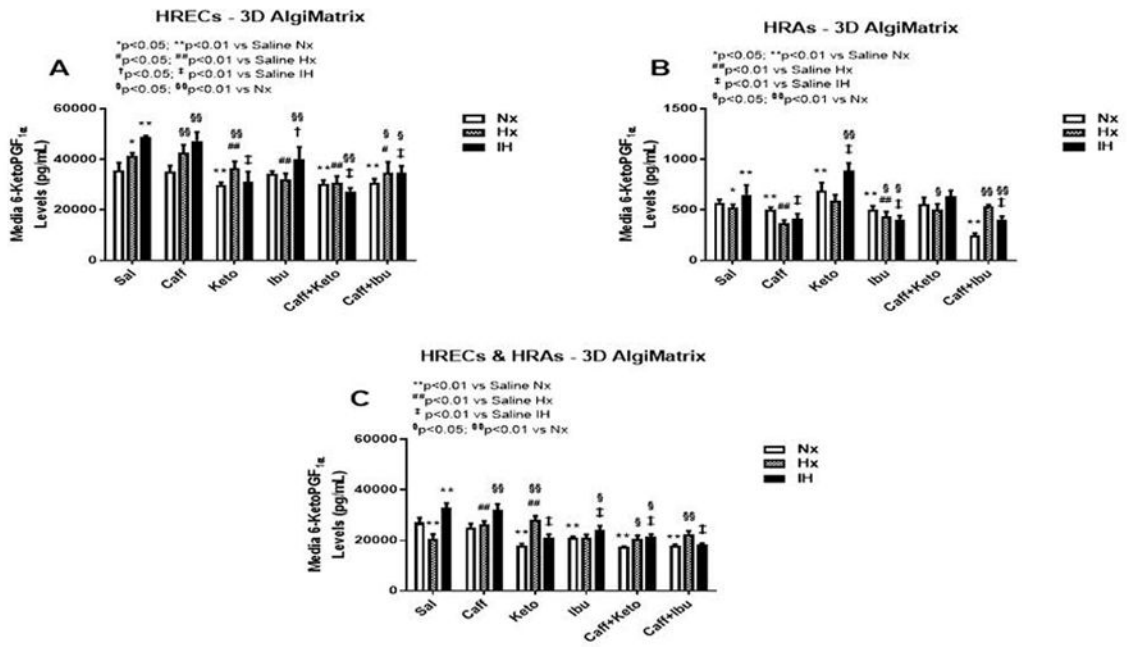


Figure 10. 6-ketoPGF_{1α} levels in media from 3-D AlgMatrix biodegradable hydrogel scaffolds. Panel A represents data from HRECs, panel B from HRAs and panel C from co-cultures of HRECs+HRAs. Data are presented as mean±SEM (n=8 samples/groups). Data are presented as mean±SEM (n=8 samples/groups). Comparison to saline Nx is represented by *p<0.05; **p<0.01; comparison to saline Hx is represented by #p<0.05; ##p<0.01; comparison to saline IH is represented by †p<0.05; ‡p<0.01; and comparison among the treated groups is represented by §p<0.05; §§p<0.01.

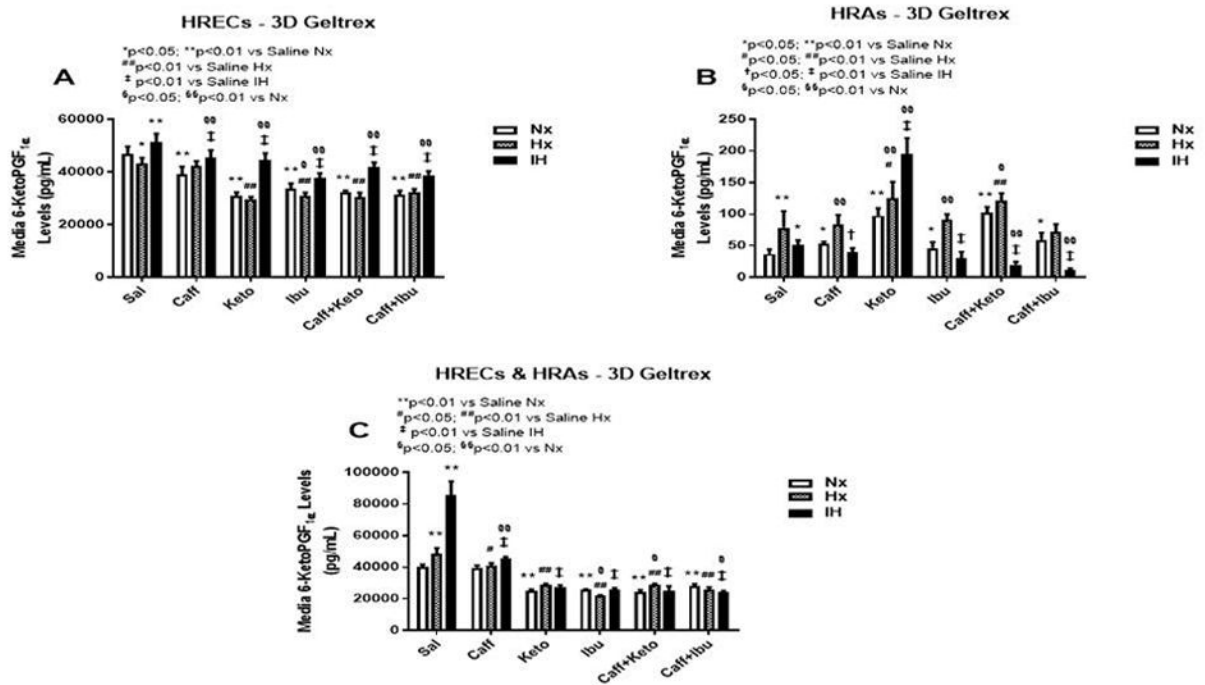


Figure 11.

6-ketoPGF_{1α} levels in media from 3-D Geltrex biodegradable hydrogel scaffolds. Panel A represents data from HRECs, panel B from HRAs, and panel C from co-cultures of HRECs +HRAs. Data are presented as mean±SEM (n=8 samples/groups). Data are presented as mean±SEM (n=8 samples/groups). Comparison to saline Nx is represented by *p<0.05; **p<0.01; comparison to saline Hx is represented by #p<0.05; ##p<0.01; comparison to saline IH is represented by †p<0.05; ‡p<0.01; and comparison among the treated groups is represented by §p<0.05; §§p<0.01.

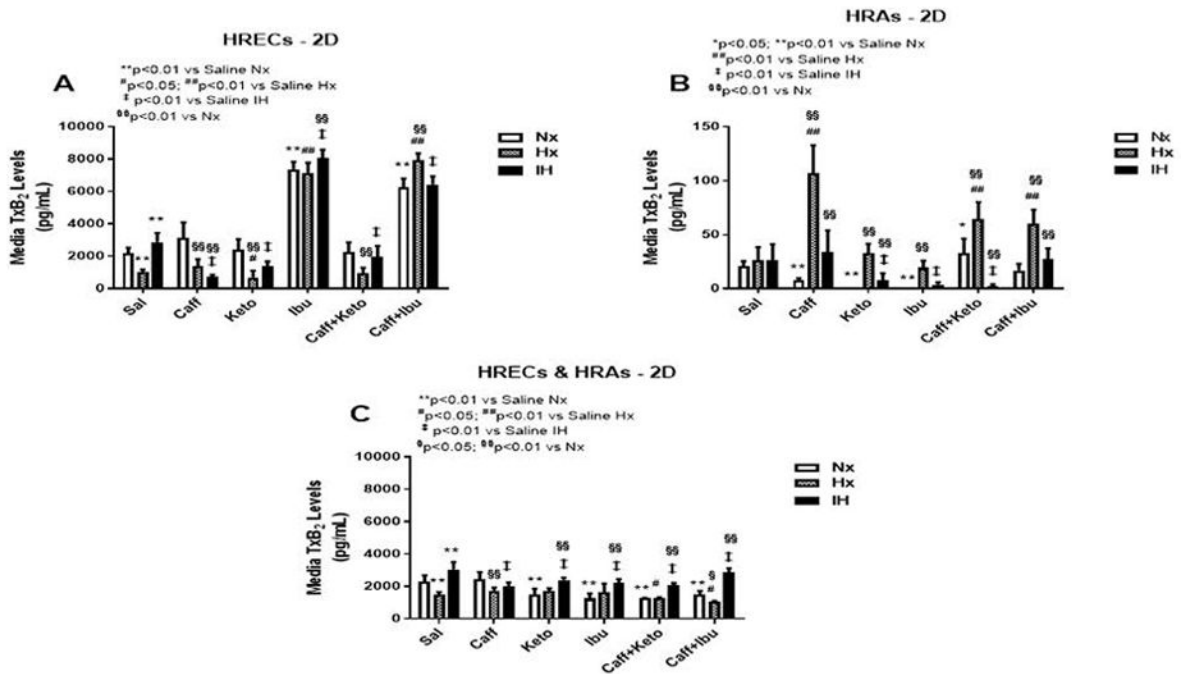


Figure 12.

TxB₂ levels in media from cells cultured on 2-D surfaces. Panel A represents data from HRECs, panel B from HRAs and panel C from co-cultures of HRECs+HRAs. Data are presented as mean±SEM (n=8 samples/groups). Comparison to saline Nx is represented by *p<0.05; **p<0.01; comparison to saline Hx is represented by #p<0.05; ##p<0.01; comparison to saline IH is represented by †p<0.05; ††p<0.01; and comparison among the treated groups is represented by §p<0.05; §§p<0.01.

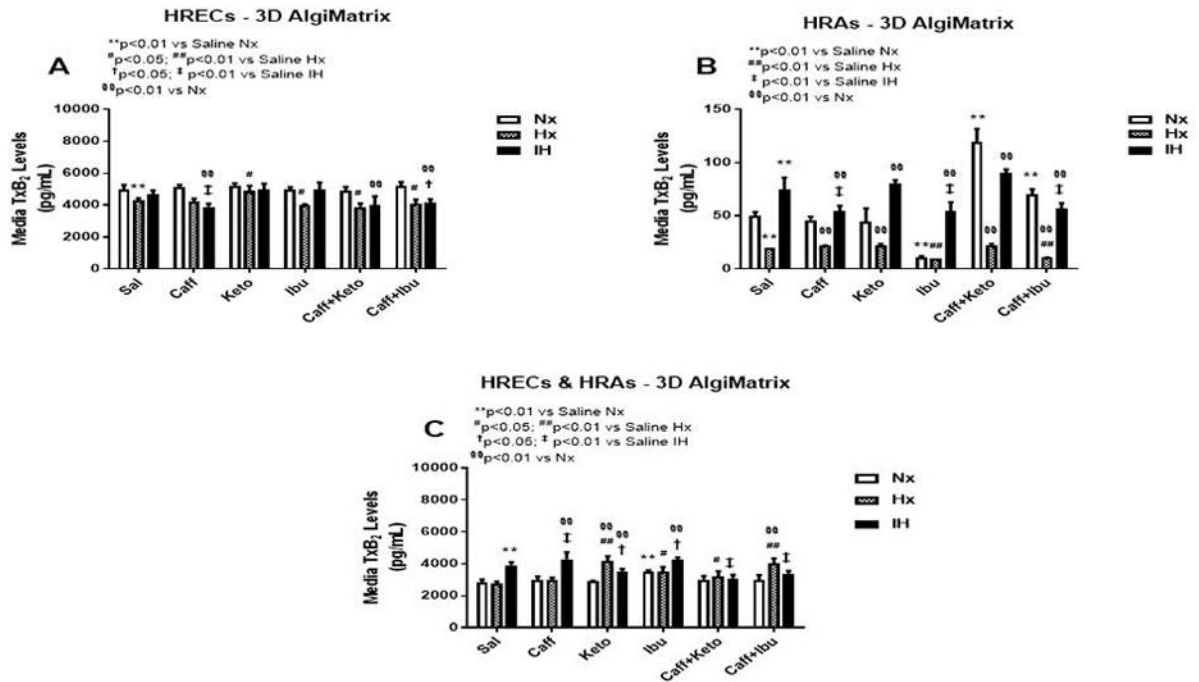


Figure 13. TxB₂ levels in media from 3-D AlgiMatrix biodegradable hydrogel scaffolds. Panel A represents data from HRECs, panel B from HRAs and panel C from co-cultures of HRECs +HRAs. Data are presented as mean±SEM (n=8 samples/groups). Data are presented as mean±SEM (n=8 samples/groups). Comparison to saline Nx is represented by *p<0.05; **p<0.01; comparison to saline Hx is represented by #p<0.05; ##p<0.01; comparison to saline IH is represented by †p<0.05; ‡p<0.01; and comparison among the treated groups is represented by §p<0.05; §§p<0.01.

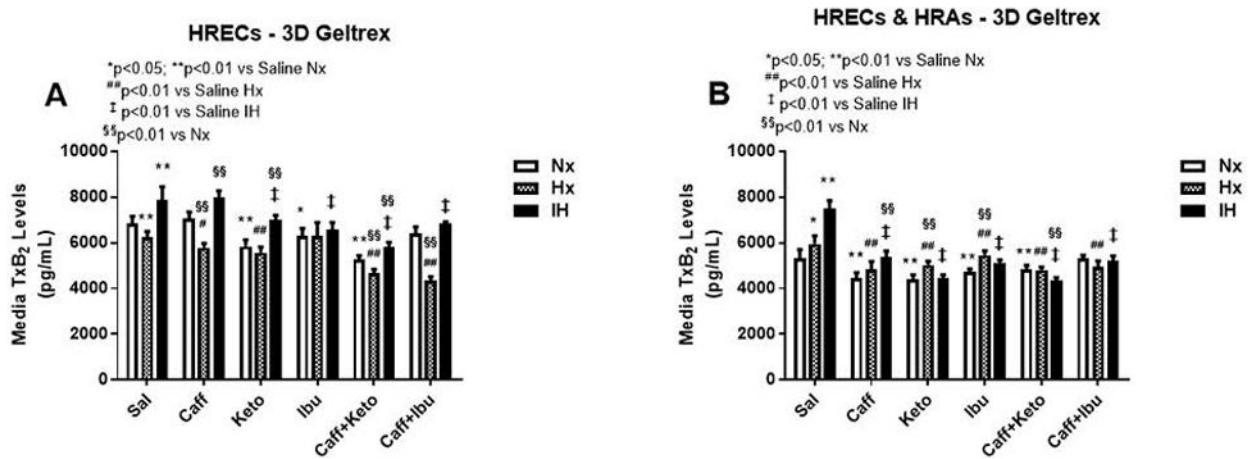


Figure 14.

TxB₂ levels in media from 3-D Geltrex biodegradable hydrogel scaffolds. Panel A represents data from HRECs, and panel B from co-cultures of HRECs+HRAs. Data are presented as mean±SEM (n=8 samples/groups). Data are presented as mean±SEM (n=8 samples/groups). Comparison to saline Nx is represented by *p<0.05; **p<0.01; comparison to saline Hx is represented by #p<0.05; ##p<0.01; comparison to saline IH is represented by †p<0.05; p<0.01

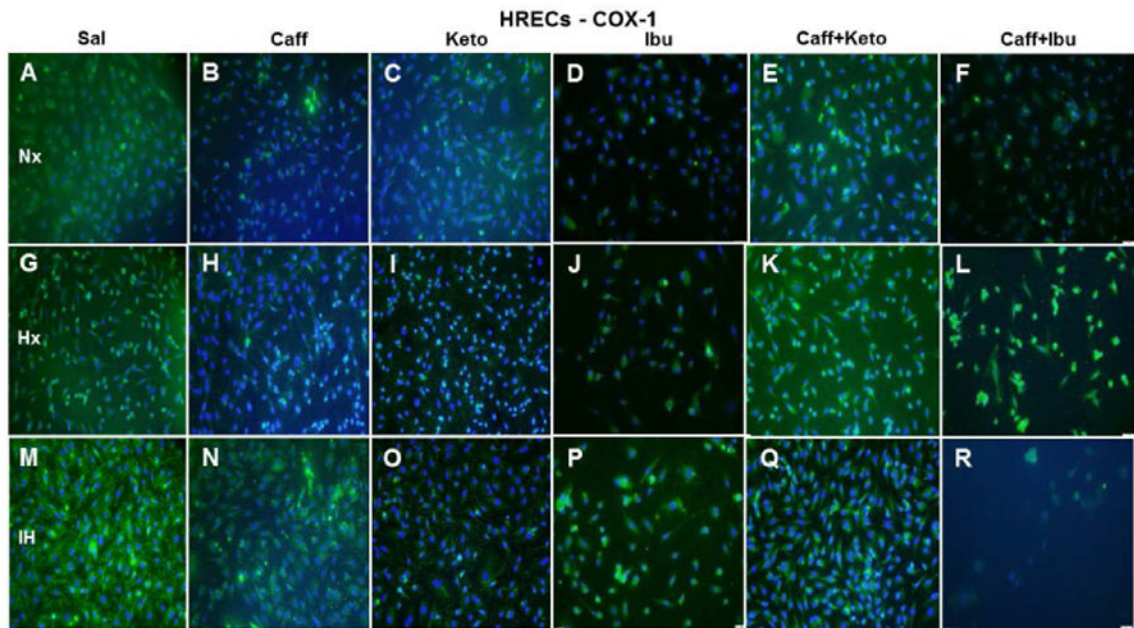


Figure 15.

Representative image of COX-1 immunoreactivity in HRECs. The green stain is COX-1 immunoreactivity and the blue color is DAPI staining of the nuclei. Panels A through F represents the Nx groups, panels G through L represents the Hx groups, and panels M through R represents the IH groups. Treatment groups are saline (Panels A, G, and M), caffeine (panels B, H, and N), ketorolac (panels C, I, and O), ibuprofen (panels D, J, and P), caffeine+ketorolac (panels E, K, and Q), and caffeine+ibuprofen (panels F, L, and R). Images are captured at 20X magnification. Scale bar is 100 μ m.

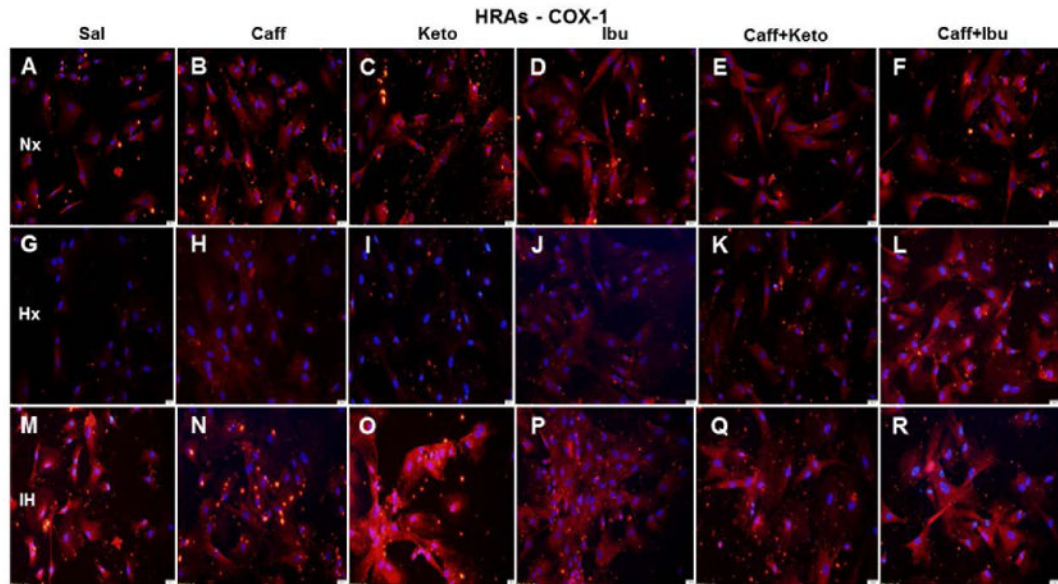


Figure 16.

Representative image of COX-1 immunoreactivity in HRAs. The red stain is COX-1 immunoreactivity and the blue color is DAPI staining of the nuclei. Groups are as described in Figure 15. Images are captured at 20X magnification. Scale bar is 100 μ m.

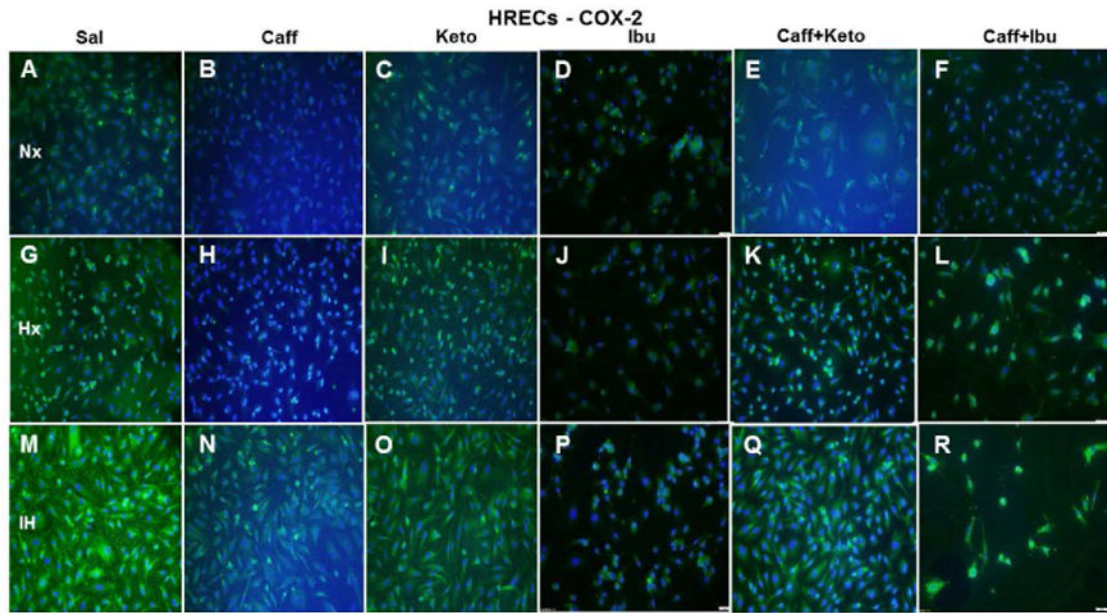


Figure 17.

Representative image of COX-2 immunoreactivity in HRECs. The green stain is COX-2 immunoreactivity and the blue color is DAPI staining of the nuclei. Groups are as described in Figure 15. Images are captured at 20X magnification. Scale bar is 100 μ m.

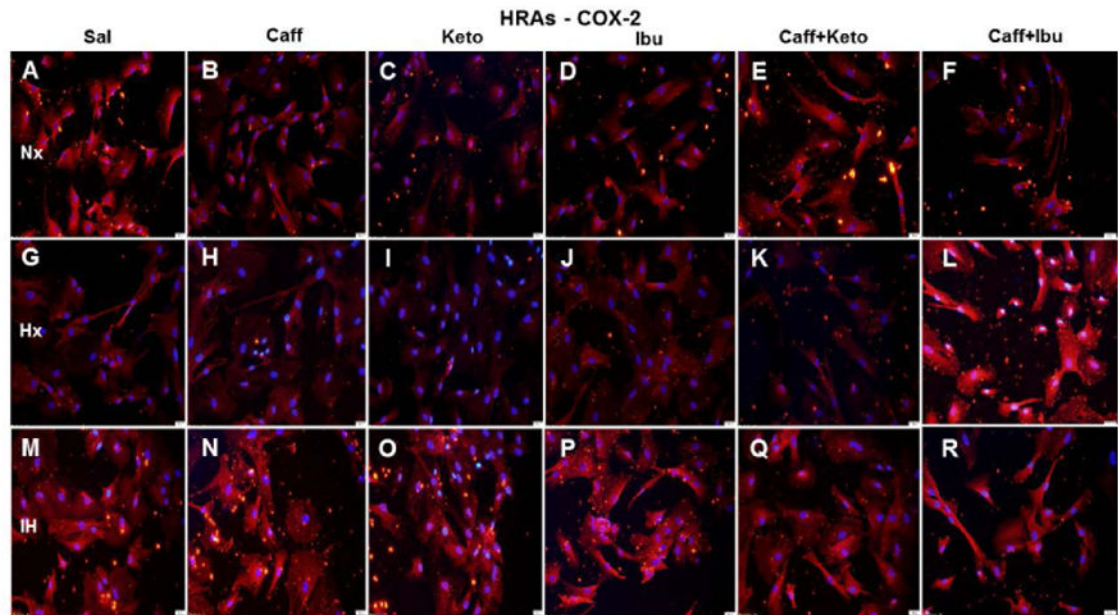


Figure 18.

Representative image of COX-2 immunoreactivity in HRAs. The red stain is COX-2 immunoreactivity and the blue color is DAPI staining of the nuclei. Groups are as described in Figure 15. Images are captured at 20X magnification. Scale bar is 100 μ m.